

NbTi: a nontrivial puzzle for the conventional theory of superconductivity

Alessio Cucciari,^{1,†} Dionisia Naddeo,^{1,*} Simone Di Cataldo,^{1,‡} and Lilia Boeri^{1,§}

¹*Dipartimento di Fisica, Sapienza - Università di Roma, 00185 Rome, Italy*

(Dated: March 27, 2024)

We present the first *ab-initio* study of superconductivity in NbTi, the workhorse for many applications. Despite its apparent simplicity, NbTi turns out to be a major challenge for computational superconductivity. In fact, anharmonic effects are crucial to obtain dynamically stable phonons for the ordered bcc phase, unstable at the harmonic level, and beyond-Morel Anderson effects in the Coulomb interaction reduce the T_c by more than 20 %. Lattice disorder causes an additional large discrepancy in T_c compared to experiment. Our results imply that a quantitative description of technologically-relevant superconductors requires methodological developments beyond the current standards.

In the last decade *ab-initio* methods based on Density Functional Theory (DFT) represented an invaluable driving force in superconducting material research, culminating in the discovery of near-ambient temperature superconductivity in high-pressure superhydrides [1–6]. Wannier-based interpolation of electron-phonon matrix elements [7], accurate functionals for the superconducting state [8], improved approximations to describe the Coulomb interaction [9, 10] and quantum lattice effects [11] are just a few of the recent developments which have enormously improved the accuracy of DFT-based methods for superconductors. Recent benchmarks show that both Superconducting Density Functional Theory (SCDFT) and *ab-initio* Migdal-Éliashberg have achieved an accuracy within 10-20% against the experimental T_c and related properties for most superconductors [8, 12]. However, a few notable exceptions have been found, where the description of superconductivity is unusually intricate: a striking example is elemental mercury [13].

In this Letter we will apply state-of-the-art *ab-initio* methods to study NbTi, a simple alloy which, due to its relatively low cost, malleability, and high critical fields is considered the workhorse material for most superconducting applications [14, 15]. Low-temperature superconductors like NbTi currently account for 75% of the current market share of superconductors; however, despite their technological relevance, they have been relatively little studied using modern computational techniques. The only recent first-principle study on NbTi employs semi-qualitative arguments to explain the pressure-dependence of T_c [16].

In this paper we show that obtaining a reliable estimate of T_c for the simplest model of NbTi, i.e. the ordered bcc- β phase, requires including non-standard effects like anharmonic lattice dynamics and energy-dependent Coulomb interactions. Even so, the calculated T_c is largely overestimated compared to experiments; using a simple model based on Boltzmann-averaged supercells we show that the discrepancy can be qualitatively understood in terms of lattice disorder. Recovering a quantitative agreement would require devising realistic

models to include lattice disorder, which go beyond the current standards of *ab-initio* theories of superconductivity.

Commercial samples of NbTi contain a mixture of several phases (α , β , ω), but it is normally assumed that superconductivity is dominated by the β -phase [17], in which Nb and Ti atoms are randomly distributed on a bcc lattice. The bcc β -phase is the only phase stable for low-Ti concentrations $x \in [0.0, 0.4]$ in the Nb_{1-x}Ti_x phase diagram [18]. For larger x , increasingly larger inclusions of the hexagonal α form until, for $x \geq 0.8$, the α phase becomes stable. T_c remains essentially constant $\simeq 9$ K from $x = 1$ until around $x = 0.4$, where it drops rapidly reaching 0.3 K in pure Ti. The maximum of T_c (9.7 K) is achieved at optimal doping $x_{opt} = 0.37$, where the critical field H_{c2} is as high as 14 T at 2 K [14, 17]. A recent study has shown that samples near optimal concentration retain superconductivity up to a pressure of 261.7 GPa, setting new records of 19.1 K for the T_c and 19 T for the H_{c2} for transition metal (TM) alloy superconductors [19].

In this work, we employed state-of-the-art *ab initio* calculations based on Density Functional Theory, the Stochastic Self Consistent Harmonic Approximation (SSCHA), and Éliashberg theory for the superconducting state [7, 11, 20–23] to study the electronic, vibrational and superconducting properties of the 1:1 ordered bcc-phase ($x = 0.5$) usually assumed to be a realistic model for near-optimal concentrations – see [24] and Section I of the Supplementary Material [25] for computational details. In this phase Nb and Ti atoms occupy alternatively the 1a and 1b Wyckoff positions of a $Pm\bar{3}m$ CsCl lattice [16]; the optimized lattice parameter at ambient pressure is 3.27 Å, to be compared with the experimental value of 3.29 Å.

The electronic structure is shown in Fig. 1. The valence bands extend ~ 6 eV below the Fermi level, where they are dominated by electronic states of Nb and Ti s and d -characters. The corresponding Density of States (DOS), reported in panel b), exhibits several sharp peaks; the Fermi level intersects the DOS at its near-maximum value $N(\epsilon_F) = 2.19$ st/eV/at for $x = 0.5$. Optimal doping ($x =$

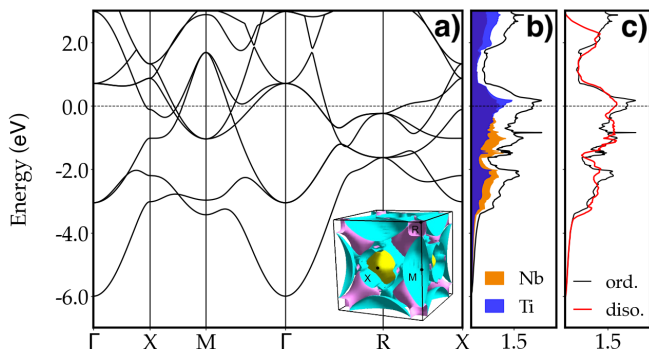


FIG. 1. **a)** Electronic band structure of β -NbTi. The inset shows the Fermi surface, with different colors denoting different bands. **b)** Atom-projected density of states (DOS) in units of states/eV/at. Projections onto Nb and Ti are shown in orange and blue, respectively. The zero of the energy is the Fermi level. **c)** In this panel, the DOS of the ordered phase is compared with that of a simple model of a disordered phase - see text.

0.37) corresponds to an upward shift of the Fermi level of around 50 meV, which leaves $N(\epsilon_F)$ almost unchanged [26]. The Fermi surface, shown in the inset of Fig. 1, comprises four sheets: two large cuboidal hole pockets centered around the Γ point and two smaller ellipsoidal pockets of electron character around the Brillouin zone edges [27]. Due to the cuboidal shape of the hole pockets, several portions of the Fermi surface are nearly parallel (nested), causing near-divergences in the non-interacting Lindhard function.

The phonon dispersions of ordered β -NbTi are shown in Fig. 2 (a). Dashed black lines represent harmonic dispersions obtained within Density Functional Perturbation Theory (DFPT) [28]. In agreement with previous calculations [16], we find that at the harmonic level bcc-NbTi is dynamically unstable and exhibits imaginary frequencies. Lattice instabilities, predicted for instance around the M points, midway along the Γ -R line and the R-X line, are very localized in momentum space. This is a typical signature of electronically-driven phonon anomalies - Kohn anomalies [29].

In fact, as indicated by the red arrows, the position of the Kohn anomalies in \mathbf{q} -space corresponds one-to-one to peaks in the imaginary part of the non-interacting Lindhard function, the so-called nesting function, shown in panel (d) of Fig. 2. Peaks in the nesting function occur whenever the same wave-vectors \mathbf{q} connect, i.e. *nest* sizable parts of the Fermi surface. Fig. 2 shows for example that the wavevector $\mathbf{q} = M$ is a nesting vector of the Fermi surface, since it connects nearly-parallel flat faces of the hole surface centered at the Γ point.

The small inset of panel a) shows the vibration pattern of one of the two modes which are unstable at the harmonic level for this particular wavevector. The mode induces a shear of the $(0\bar{1}1)$ planes of the bcc crystal,

in alternate $[011]$ and $[0\bar{1}\bar{1}]$ directions. This is the Burgers' deformation path for the $\beta \rightarrow \alpha$ (bcc to hexagonal) transition [30–32], which in $\text{Nb}_{1-x}\text{Ti}_x$ is experimentally observed at low temperatures for $x > 0.8$. For near-optimal concentrations ($x \sim 0.5$), the Burgers' transition is not observed, and the bcc phase remains stable at all temperatures [17].

Indeed, our calculations show that dynamical instabilities predicted at the harmonic level for $x = 0.5$ are eliminated if lattice dynamics are described with a method which includes phonon-phonon interactions. In this work we employed a recent implementation of the Stochastic Self-Consistent Harmonic Approximation which relies on Machine Learning Interatomic Potentials (SSCHA-MLIP [33]), which ensures an optimal convergence of dynamical matrices and phonon dispersions with respect both to the number of structures sampled and supercell size. [34]. Solid black lines in Fig. 2 (a) represent results of fully anharmonic SSCHA-MLIP calculations [35]: anharmonic effects remove the lattice instabilities at the harmonic level and the residual effect of Kohn anomalies is a \mathbf{q} -dependent phonon softening.

The sizable anharmonic renormalization of the phonon dispersions in NbTi is strongly related to the anharmonic suppression of charge density wave instabilities observed, for instance, in transition metal dichalcogenides [36]. In

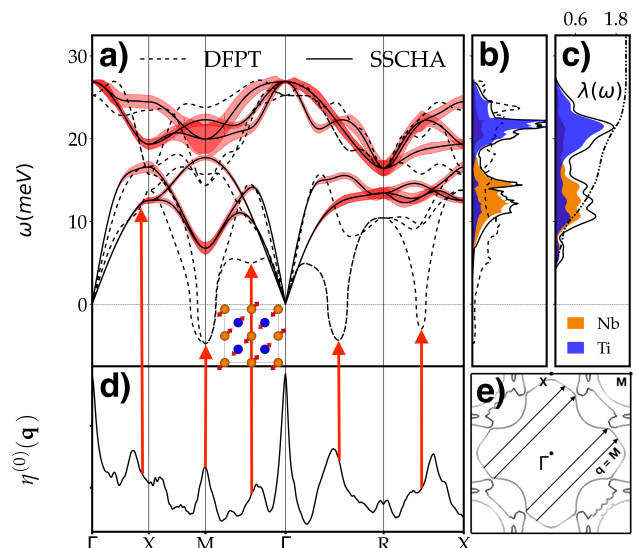


FIG. 2. **a)** Anharmonic (full black lines) phonon dispersions of the ordered β -NbTi, decorated with their linewidths (red shading). The corresponding harmonic phonons are represented by dashed black lines. The inset shows the vibration pattern of one of the two unstable eigenmodes at the M point. **b)** Atom-projected and total phonon density of states in units of states/meV. **c)** Atom-projected and total Éliashberg spectral function, along with the electron-phonon coupling $\lambda(\omega)$ (dotted black line) **d)** Nesting function $\eta^{(0)}(\mathbf{q})$. Red arrows highlight the position of Kohn anomalies. **e)** Projection of the Fermi surface onto the $[110]$ lattice plane; black arrows indicate parts of the Fermi surface which contribute to the peak in the nesting functions for $\mathbf{q} = M$.

both types of systems, sizeable anharmonic effects become relevant not because atoms with a light mass sample anharmonic regions of the potential corresponding to large displacements, as in hydrides [37–39], but because near-divergent electronic susceptibilities make the phonon potential anharmonic already at small displacements [40].

To compute the superconducting properties of β -NbTi, we employed the SSCHA dynamical matrices and the electron-phonon matrix elements (calculated from the anharmonic phonon eigenvectors) computed on coarse \mathbf{k} - and \mathbf{q} -grids in reciprocal space, that were subsequently Wannier-interpolated on denser grids [7, 23] to obtain phonon frequencies $\omega_{\mathbf{q}\nu}$ and linewidths $\gamma_{\mathbf{q}\nu}$, from which the Éliashberg spectral function $\alpha^2 F(\omega)$ was obtained as:

$$\alpha^2 F(\omega) = \frac{1}{2\pi N(\epsilon_F)} \sum_{\mathbf{q}\nu} \frac{\gamma_{\mathbf{q}\nu}}{\omega_{\mathbf{q}\nu}} \delta(\omega - \omega_{\mathbf{q}\nu}) \quad (1)$$

The *anharmonic* $\alpha^2 F(\omega)$, shown in panel *c*) of Fig. 2, closely follows the shape of the phonon DOS, shown in panel *b*) of the same figure. Indeed, phonon linewidths, shown as red shading of the phonon dispersions, are distributed uniformly across the whole spectrum.

The phonon spectrum extends up to 28 meV, with two large peaks centered at around 15 meV and 25 meV, corresponding mainly to Nb and Ti vibrations. It is impossible to compare the calculated spectrum with experiments, since no inelastic neutron scattering or tunneling data are available for NbTi. However, both the phonon DOS and the Eliashberg functions resemble closely the data available for pure Nb, which has the same bcc crystal structure as NbTi and a very similar T_c of 9.3 K [41].

Solving the anisotropic Migdal–Éliashberg equations in the full-bandwidth approximation, as implemented in the EPW code [7, 42], we obtained the superconducting gap as a function of temperature, shown as red dashed line in Fig. 3. The extrapolated value of T_c is 24.3 K [43], while for the isotropic gap (black dashed line) we obtain a slightly lower value of T_c (23.7 K). These values were obtained approximating the residual Coulomb interaction between electrons with a Morel-Anderson pseudopotential $\mu^* = 0.20$.

This value, obtained screening the static screened interaction computed in the Random-Phase Approximation (details in the SM), is consistent with a similarly large value obtained by Pellegrini et al. for pure Nb [44]. In the same paper, the authors have shown that, due to the strong localization of *d* states, treating Coulomb interactions beyond the μ^* approximation, i.e. in the full-RPA and beyond-RPA Kukkonen-Overhauser framework, progressively improves the agreement between theoretical and experimental T_c 's [10, 45] – see the second line of table I.

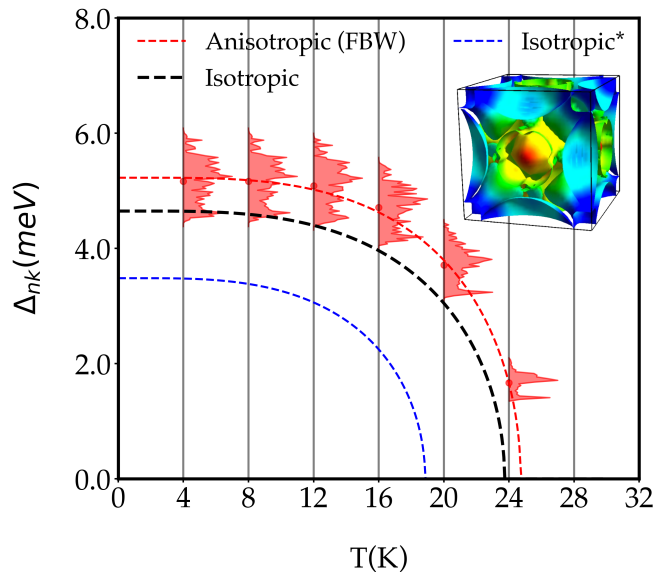


FIG. 3. Energy distribution of the zero-frequency superconducting gap of ordered β -NbTi as a function of temperature, obtained solving the anisotropic Migdal–Éliashberg equations for $\mu^* = 0.20$. The distribution of the superconducting gap over the Fermi surface is reported in the inset with a color scale which goes from the minimum to the maximum value of the gap (4.5 to 5.8 meV). Dashed lines indicate a fit of the weighted averages of the distribution for each T in red, the corresponding isotropic solution in black, and the isotropic solution for the disordered model in blue.

Also in NbTi using progressively more accurate approximations for the Coulomb interactions reduces T_c by around 20 %, down to 19 K in the KO approximation. However, at variance with Nb, in this case the agreement between calculations and experiments is far from satisfactory: the calculated T_c is still twice as large as the experimental one, whereas typical errors in T_c 's for modern *ab-initio* methods for superconductivity are of the order of 10-20 % [8, 12].

We can try to retrace the source of this anomalously large discrepancies by comparing the main electron-phonon parameter of Nb and NbTi, reported in the first two rows of table I. We see that while the values of ω_{log} are comparable, the electron-phonon coupling constant λ of NbTi is 1.5 times as large as in pure Nb, reflecting a similar difference in the value of the DOS at the Fermi level. Indeed, the high value of $N(\epsilon_F)$ we predict for NbTi may be an artifact of assuming a perfectly ordered alloy, whereas in actual samples Nb and Ti atoms are randomly distributed on crystal lattice sites. The typical effect of disorder is to “smear out” sharp features in the electronic DOS and nesting function and hence reduce the magnitude and the concentration-dependence of the T_c .

	$N(\epsilon_F)$	ω_{log}	λ	$T_c^{\mu^*}$	T_c^{RPA}	T_c^{KO}	T_c^{exp}
NbTi	2.19	14.4	1.87	23.7	21.4	19.0	9.7
Nb	1.42	12.0	1.34	14.1	12.4	11.0	9.3
NbTi*	1.77	14.4	1.48	18.9	16.7	14.3	9.7

TABLE I. Superconducting properties of Nb and NbTi alloys. $N(\epsilon_F)$ is the Density of States at the Fermi level in states/ev/at; ω_{log} is the logarithmically-averaged phonon frequency in meV; λ is the total electron-phonon coupling parameter. The various T_c in K were obtained solving the isotropic Migdal-Eliashberg equations using increasingly more accurate approximations for the Coulomb interaction, i.e. the Morel-Anderson μ^* approximation [46], the full energy-dependent RPA kernel [44], and the Kukkonen-Overhauser scheme [10, 45]. Data for pure Nb are from Refs [8, 47]. NbTi and NbTi* indicate results for the ordered bcc lattice and for the disorder-rescaled model (see text).

In order to obtain a qualitative estimate of the effect of disorder on the superconducting properties of NbTi, we performed a simple *gedanken* experiment, fixing the shape of the Eliashberg function and of the Coulomb interaction to that of the ordered bcc crystal and rescaling their amplitude by the DOS at the Fermi level of a model disordered crystal. The DOS of the disordered NbTi crystal was simulated performing a Boltzmann-average of the DOS of 100 randomly-generated $2 \times 2 \times 2$ supercells with 1:1 stoichiometry [48]. The energies of all randomly-generated supercells were in fact down to 60 meV/atom lower than that of ordered crystal, indicating that a randomly disordered crystal may be a more realistic assumption than the perfectly ordered alloy. The Boltzmann-averaged DOS is shown as red dashed lines in panel c) of Fig. 1. As expected, disorder smoothens many of the sharp features of the ordered DOS; as a result the $N(\epsilon_F)$ decreases by 20%, from 2.19 down to 1.77 st/eV/at.

Solving the Eliashberg equations with the rescaled model, we obtain the results shown in the last row of Table I (NbTi*). The T_c in the KO approximation is reduced to 14.3 K, in satisfactory agreement with experiment, given our crude approximation for disorder. Some of us have recently proposed that a similar DOS smoothing effect may explain the weak pressure-dependence of T_c in bcc Ti at extreme pressures [49], although in that case the underlying physical mechanism is based on vacancies rather than disorder. Both results indicate that the superconducting properties of Ti-rich alloys may be strongly affected by the presence of lattice imperfections. These types of effects are quite hard to quantify in first-principles calculations.

In conclusion, in this work we investigated the superconducting properties of the workhorse superconductor NbTi, using state-of-the-art *ab-initio* methods. We showed that, despite the apparent simplicity of this ma-

terial, the description of the ordered bcc β -phase, commonly assumed as a model for the optimally-doped crystal, presents several challenges for state-of-the-art computational methods: (i) Lattice dynamics has to be treated in a fully anharmonic framework to remove the dynamical instabilities associated to Kohn anomalies, which prevented the calculations of T_c in previous studies [16]; (ii) Coulomb interactions beyond the standard Morel-Anderson μ^* approximation have a non-negligible effect on T_c , reducing the calculated values by more than 20%; (iii) This is however not enough to bring the calculated T_c 's in agreement with experiment, since neglecting lattice disorder leads to a strong overestimation of the DOS at the Fermi level, and hence T_c . Lattice disorder, which in this work was treated with a simple ad-hoc model based on Boltzmann-averaged supercells, seems to play a major role in many Ti-rich systems, which exhibit a weak dependence of T_c on external parameters such as composition and pressure [16, 19, 49]. Incorporating qualitatively the effects of lattice disorder is well beyond the capabilities of current first-principles theories of superconductivity. However, this may be essential for a real coming-of-age of the field, as realistic modelling of technologically-relevant superconductors is arguably one of the essential future challenges in the field.

Acknowledgments: The authors would like to thank C.Heil, E. Kogler, R. Lucrezi for help with the SSCHA-MLIP calculations, and A. Sanna for discussion and for performing the calculations of the Coulomb interaction beyond the μ^* approximation. We would also like to thank Alex Gurevich and David Larbastier for useful discussion on NbTi literature.

The authors acknowledge computational resources from CINECA, projects IsC90-HTS-TECH and IsC99-ACME-C, and the Vienna Scientific Cluster, project 71754 "TEST". L.B. acknowledges support from Fondo Ateneo Sapienza 2019-22, and funding from the European Union - NextGenerationEU under the Italian Ministry of University and Research (MUR), "Network 4 Energy Sustainable Transition - NEST" project (MIUR project code PE000021, Concession Degree No. 1561 of October 11, 2022) - CUP C93C22005230007.

† alessio.cucciari@uniroma1.it

* naddeo.1749354@studenti.uniroma1.it

‡ simone.dicataldo@uniroma1.it

§ lilia.boeri@uniroma1.it

- [1] D. Duan, Y. Liu, F. Tian, D. Li, X. Huang, Z. Zhao, H. Yu, B. Liu, W. Tian, and T. Cui, Scientific Reports **4**, 6968 (2014).
- [2] A. Drozdov, M. Eremets, I. Troyan, *et al.*, Nature **525**, 73 (2015).
- [3] H. Liu, I. I. Naumov, R. Hoffmann, N. W. Ashcroft, and R. J. Hemley, Proceedings of the National Academy of

- Sciences **114**, 6990 (2017).
- [4] A. P. Drodzov, P. P. Kong, S. P. Besedin, M. A. Kuzonikov, S. Mozaffari, L. Balicas, F. F. Balakirev, D. E. Graf, V. B. Prakapenka, E. Greenberg, D. A. Knyazev, M. Tkacz, and M. I. Eremets, *Nature* **569**, 528 (2019).
- [5] M. Somayazulu, M. Ahart, A. K. Mishra, Z. M. Geballe, M. Baldini, Y. Meng, V. V. Struzhkin, and R. J. Hemley, *Phys. Rev. Lett.* **122**, 027001 (2019).
- [6] J. A. Flores-Livas, L. Boeri, A. Sanna, G. Profeta, R. Arita, and M. Eremets, *Physics Reports* **856**, 1 (2020).
- [7] S. Poncé, E. R. Margine, C. Verdi, and F. Giustino, *Comp. Phys. Communications* **209**, 116 (2016).
- [8] A. Sanna, C. Pellegrini, and E. K. U. Gross, *Phys. Rev. Lett.* **125**, 057001 (2020).
- [9] A. Davydov, A. Sanna, C. Pellegrini, J. K. Dewhurst, S. Sharma, and E. K. U. Gross, *Phys. Rev. B* **102**, 214508 (2020).
- [10] C. Pellegrini, C. Kukkonen, and A. Sanna, *Phys. Rev. B* **108**, 064511 (2023).
- [11] L. Monacelli, R. Bianco, M. Cherubini, M. Calandra, I. Errea, and F. Mauri, *J. Phys. Condens. Matter* **33**, 363001 (2021).
- [12] M. Kawamura, Y. Hizume, and T. Ozaki, *Phys. Rev. B* **101**, 134511 (2020).
- [13] C. Tresca, G. Profeta, G. Marini, *et al.*, *Phys. Rev. B* **106**, L180501 (2022).
- [14] R. Scanlan, A. Malozemoff, and D. Larbalestier, *Proceedings of the IEEE* **92**, 1639 (2004).
- [15] K. Kinoshita, *Phase Transitions* **23**, 73 (1990).
- [16] J.-F. Zhang, M. Gao, K. Liu, and Z.-Y. Lu, *Phys. Rev. B* **102**, 195140 (2020).
- [17] E. Collings, *A sourcebook of titanium alloy superconductivity* (Springer Science & Business Media, 2012).
- [18] In this work alloy compositions are specified in atomic percent, rather than weight percent. Thus, x indicates the fraction of Ti atoms/f.u.
- [19] J. Guo, G. Lin, S. Cai, C. Xi, C. Zhang, W. Sun, Q. Wang, K. Yang, A. Li, Q. Wu, Y. Zhang, T. Xiang, R. J. Cava, and L. Sun, *Advanced Materials* **31**, 1807240 (2019).
- [20] P. Giannozzi, S. Baroni, N. Bonini, M. Calandra, R. Car, C. Cavazzoni, D. Ceresoli, G. L. Chiarotti, M. Cococcioni, and I. Dabo, *J. Phys.: Condens. Matter* **21**, 395502 (2009).
- [21] P. Giannozzi, O. Andreussi, T. Brumme, O. Bunau, M. B. Nardelli, M. Calandra, R. Car, C. Cavazzoni, D. Ceresoli, M. Cococcioni, N. Colonna, I. Carnimeo, A. D. Corso, S. de Gironcoli, P. Delugas, R. A. DiStasio, A. Ferretti, A. Floris, G. Fratesi, G. Fugallo, R. Gebauer, U. Gerstmann, F. Giustino, T. Gorni, J. Jia, M. Kawamura, H.-Y. Ko, A. Kokalj, E. Küçükbenli, M. Lazzeri, M. Marsili, N. Marzari, F. Mauri, N. L. Nguyen, H.-V. Nguyen, A. O. de-la Roza, L. Paulatto, S. Poncé, D. Rocca, R. Sabatini, B. Santra, M. Schlipf, A. P. Seitsonen, A. Smogunov, I. Timrov, T. Thonhauser, P. Umari, N. Vast, X. Wu, and S. Baroni, *J. Phys.: Condens. Matter* **29**, 465901 (2017).
- [22] I. Errea, M. Calandra, and F. Mauri, *Phys. Rev. B* **89**, 064302 (2014).
- [23] F. Giustino, M. L. Cohen, and S. G. Louie, *Phys. Rev. B* **76**, 165108 (2007).
- [24] Electronic and vibrational properties were computed within Density Functional Perturbation Theory (DFPT) in a plane-wave and pseudopotential framework, as implemented in the Quantum ESPRESSO (QE) suite [20, 28]. The wave functions expansion was performed with a kinetic energy cutoff of 90.0 Ry. We employed the scalar-relativistic version of Optimized Norm-conserving Vanderbilt (ONCV) pseudopotentials [50], with a Perdew-Burke-Ernzerhof (PBE) exchange-correlation functional [51]. The integration over the Brillouin zone was carried out using a regular $14 \times 14 \times 14$ Γ -centered Monkhorst-Pack [52] grid for electrons, with a Methfessel-Paxton smearing of width 0.01 Ry [53], and a $6 \times 6 \times 6$ mesh for phonons.
- [25] The Supplementary Material [URL_will_be_inserted_by_publisher] contains further computational details on the *ab-initio* calculations, as well as additional figures for the electronic structure, comparison between SSCHA-calculated phonon dispersions, details on MLIP training, on the estimate of disorder through the Boltzmann average.
- [26] See also Sect. II and Fig. 1 of the Supp. Mat. [25].
- [27] A band-by-band decomposition of the Fermi surface is reported in Fig. 2 of the Supplemental Material.
- [28] S. Baroni, S. de Gironcoli, A. D. Corso, and P. Giannozzi, *Rev. Mod. Phys.* **73**, 515 (2001).
- [29] W. Kohn, *Phys. Rev. Lett.* **2**, 393 (1959).
- [30] W. Burgers, *Physica* **1**, 561 (1934).
- [31] H. Djohari, F. Milstein, and D. Maroudas, *Phys. Rev. B* **79**, 174109 (2009).
- [32] G. Grimvall, B. Magyari-Köpe, V. Ozoliņš, and K. A. Persson, *Rev. Mod. Phys.* **84**, 945 (2012).
- [33] R. Lucrezi, E. Kogler, S. Di Cataldo, *et al.*, *Communications Physics* **6** (2023), 10.1038/s42005-024-01528-6.
- [34] See also Sect. IV and V of the Supplementary Material.
- [35] The results shown in the figure were obtained for $T=0$ K, but temperature has only a minor effect on the dispersions – See Sect. IV of the Supplementary Material.
- [36] M. Leroux, I. Errea, M. Le Tacon, S.-M. Souliou, G. Garbarino, L. Cario, A. Bosak, F. Mauri, M. Calandra, and P. Rodière, *Phys. Rev. B* **92**, 140303 (2015).
- [37] I. Errea, M. Calandra, C. J. Pickard, J. R. Nelson, R. J. Needs, Y. Li, H. Liu, Y. Zhang, Y. Ma, and F. Mauri, *Nature* **532**, 81 (2016).
- [38] M. Borinaga, I. Errea, M. Calandra, F. Mauri, and A. Bergara, *Phys. Rev. B* **93**, 174308 (2016).
- [39] I. Errea, F. Belli, L. Monacelli, A. Sanna, T. Koretsune, T. Tadano, R. Bianco, M. Calandra, R. Arita, F. Mauri, and J. A. Flores-Livas, *Nature* **578**, 66 (2020).
- [40] L. Boeri, G. Bachelet, E. Cappelluti, and L. Pietronero, *Phys. Rev. B* **65**, 214501 (2002).
- [41] E. L. Wolf, *Principles of Electron Tunneling Spectroscopy* (Oxford University Press, 2011).
- [42] R. Lucrezi, P. P. Ferreira, S. Hajmazar, *et al.*, *Communications Physics* **7** (2024), 10.1038/s42005-024-01528-6.
- [43] See Sect. VII of the Supplementary Material for details on the extrapolation.
- [44] C. Pellegrini, R. Heid, and A. Sanna, *Journal of Physics: Materials* **5**, 024007 (2022).
- [45] C. A. Kukkonen and A. W. Overhauser, *Phys. Rev. B* **20**, 550 (1979).
- [46] P. Morel and P. W. Anderson, *Physical Review* **125**, 1263 (1962).
- [47] C. Pellegrini and A. Sanna, *Personal Communications* (2024).

- [48] See Sect. VIII and Fig. 8 and 9 of the Supplementary Material [25].
- [49] A. Sanna, C. Pellegrini, S. di Cataldo, G. Profeta, and L. Boeri, Phys. Rev. B **108**, 214523 (2023).
- [50] D. R. Hamann, Phys. Rev. B **88**, 085117 (2017).
- [51] J. P. Perdew, K. Burke, and M. Ernzerhof, Phys. Rev. Lett. **77**, 3865 (1996).
- [52] H. J. Monkhorst and J. D. Pack, Phys. Rev. B **13**, 5188 (1976).
- [53] M. Methfessel and A. T. Paxton, Phys. Rev. B **40**, 3616 (1989).